Repetitive Hibernation-Like State Suppresses the Progression of Amyloid Pathology

Ikumi Oomoto[1], Yong Huang[1], Maya Odagawa[1], Takeshi Sakurai[2,3,4], Genshiro A. Sunagawa[5], Hiroki Sasaguri[6], Masanori Murayama[1]
1. Laboratory for Haptic Perception and Cognitive Physiology, RIKEN Center for Brain Science, Wako-shi 351-0198, Saitama, Japan.
2. Institute of Medicine, University of Tsukuba, Tsukuba, 305-8575 Ibaraki, Japan.
3. International Institute for Integrative Sleep Medicine (WPI-IIIS), Tsukuba Institute for Advanced Research (TIAR), University of Tsukuba, Tsukuba, 305-8575 Ibaraki, Japan.
4. Life Science Center for Tsukuba Advanced Research Alliance, University of Tsukuba, Tsukuba, 305-8577 Ibaraki, Japan.
5. Laboratory for Hibernation Biology, RIKEN Center for Biosystems Dynamics Research, Kobe-shi, 650-0047 Hyogo, Japan.
6. Dementia Pathophysiology Collaboration Unit, RIKEN Center for Brain Science, Wako-shi 351-0198, Saitama, Japan.

Abstract

Alzheimer's disease (AD) is known to exhibit amyloid pathology years before the onset of cognitive impairment. While early detection and pathological modification are considered essential for suppressing or preventing disease progression, effective strategies remain elusive. Here, we investigated whether inducing a hibernation-like state via Q neuron-induced hypometabolism/hypothermia state (QIH) suppresses the progression of early amyloid pathology in AD model mice. To maximize the total duration of QIH, we established and implemented a repetitive QIH (rQIH) protocol. Using 82E1 antibody immunostaining, we found that rQIH significantly reduced early amyloid plaque burden, and the magnitude of this suppression was positively correlated with rQIH duration. rQIH also decreased the formation of dystrophic neurites surrounding plaques. These findings demonstrate that a hibernation-like physiological state can attenuate early amyloid pathology, providing a potential foundation for future hibernation-based therapeutic strategies for AD.

Keywords

hypothermia; hypometabolism; hibernation-like; amyloid plaque; Alzheimer’s disease; amyloid-beta (Aβ); amyloid pathology; animal model;

Introduction

Alzheimer's disease (AD) is one of the most pressing global health challenges, with the number of patients increasing rapidly due to aging populations. Despite decades of research, modifying the disease course or preventing progression remains difficult and continues to be a significant and unresolved issue. The central pathological feature in the early stages of AD is the extracellular accumulation of amyloid-β (Aβ) peptides resulting from the inappropriate cleavage of the amyloid precursor protein (APP). This inappropriate cleavage generates the Aβ42 form, which is prone to aggregation, accumulates, and forms toxic extracellular plaques (Hampel et al., 2021; Selkoe & Hardy, 2016). Notably, amyloid pathology typically precedes the onset of cognitive decline by many years, emphasizing the importance of identifying strategies to suppress or delay early Aβ deposition (Frisoni et al., 2022; Jack et al., 2010; Rafii & Aisen, 2023). Approaches capable of modifying these early pathological processes may hold substantial therapeutic potential for preventing or slowing AD progression. Accumulating evidence supports the hypothesis that Aβ production and accumulation are closely linked to neuronal activity and brain metabolic demand. Synaptic activity directly enhances extracellular Aβ release (Cirrito et al., 2005, 2008), and brain regions with higher lifetime metabolic rates show preferential amyloid deposition (Oh et al., 2016). Therefore, reductions in neuronal activity or metabolic demand may attenuate early amyloid pathology.

Hibernation is a physiological state characterized by reduced neuronal activity and metabolic demand, enabling animals to survive harsh environmental conditions. During hibernation, animals enter a state characterized by profound decreases in body temperature and metabolic rate, along with the suppression of physiological functions (CAREY et al., 2003; Staples, 2014). These changes help minimize energy consumption during prolonged periods of resource shortages. Importantly, recent research indicates that hibernation provides potent neuroprotection, preserving neuronal structure and function despite extreme physiological stress. (Dave et al., 2012; Zhou et al., 2001). These protective effects have stimulated interest in the concept of "hibernation-based therapies." This concept aims to harness the key mechanisms of natural hibernation to protect the brain during disease or injury.

Recent advances have revealed that activation of a specific population of hypothalamic neurons, known as QRFP-producing neurons (hereafter Q neurons), can induce a reversible, hibernation-like hypometabolic and hypothermic state, termed Q neuron-induced hypothermia/hypometabolism (QIH), in non-hibernating mammals (Takahashi et al., 2020). QIH recapitulates several features of natural hibernation, including reduced metabolic demand and lowered body temperature, without requiring a genetic or evolutionary predisposition for hibernation. Recently, the therapeutic potential of QIH in brain injury has been reported (Sakurai et al., 2025).

Given the early onset of amyloid pathology in AD and the strong neuroprotective properties of hibernation, QIH at the very earliest stage of amyloid pathology emergence might provide a unique model to examine whether hypometabolic brain states or hypothermia can modulate Aβ production, aggregation, or clearance. Here, we investigated the effect of QIH on amyloid pathology in an AD model mouse that exhibits human AD patients-like amyloid pathology at early age (Sato et al., 2021). By combining repetitive chemogenetic activation

of hypothalamic Q neurons with histological and quantitative analyses of Aβ deposition, we demonstrated that inducing a hibernation-like state can attenuate or delay the progression of amyloid plaque accumulation. Our findings provide new insights into the interplay between metabolic state and AD pathology and highlight the potential of synthetic torpor as a novel therapeutic framework for modifying disease processes associated with AD.

Results

Generation of Q-AD Tg mice and experimental scheme of repetitive QIH

To study the effect of hibernation-like behavior on the amyloid pathology, we generate a new transgenic mouse, triple-mutant Q-AD mouse, by crossbredding two different transgenic mice; one is the Qrfp^{iCre} mouse (Takahashi et al., 2020, Nature), in which we can induce QIH by activating Q neurons, the other is a third-generation AD model mouse (Sato et al., 2021), which is double-mutant of *App*$^{NL-F}$ and *Psen1*^{P117L}, and exhibits aggressive phenotype in amyloid pathology (Fig. 1A). We note that the triple-mutant mice used in this study were heterozygous for Qrfp^{iCre} and homozygous for other two genes. Q-AD mice exhibit amyloid pathology at a very early age, starting from the cortex at 6 weeks old (Fig. 1B to D, Supplementary Fig. 1), similar to the original *App*$^{NL-F}$*Psen1*^{P117L} mice (Sato et al., 2021). In the early stage (6-8 weeks), small Aβ plaques begin to appear in the deep layers of the lateral cortex. As the mice aged, plaque size gradually increased and became visible throughout the cortex. Since amyloid pathology was clearly observed in the somatosensory cortex from the earliest stages, we primarily quantified Aβ deposition in this region.

To chemogenetically activate Qfrp neurons, which leads to QIH in Q-AD mice by intraperitoneal (IP) injection of clozapine-N-oxide (CNO) (a DREADD agonist), we expressed hM3Dq–mCherry in AVPe (Anteroventral periventricular nucleus) and MPA (Medial preoptic area) by injecting 6-week-old Q-AD mice with AAV9-hSyn-DIO-hM3Dq-mCherry (Fig. 1E). The IP administration of CNO immediately induced hypothermia in QIH(+) mice, lowering their body temperature to room temperature levels (Fig. 1F and G). On average, QIH sustained around 24-36 hours upon single CNO administration in our protocol (Fig. 1G). Because mice are not natural hibernators, they do not undergo pre-hibernation metabolic adaptation or energy storage; consequently, prolonged QIH induction may lead to negative energy balance and body weight loss, imposing an excessive metabolic burden and requiring recovery periods to allow physiological re-equilibration following sustained hypometabolic states. To achieve prolonged QIH within a non-harmful range for mice, we employed a repetitive QIH (rQIH) paradigm, in which QIH was induced twice per week for either 1 month or 2 months, so that QIH could be induced for about half of the rQIH period (Fig. 1H). Repeating administration of CNO did not affect the duration of the QIH (Fig. 1I), but slightly affected the body weight in some animals (Supplementary Fig. S2).

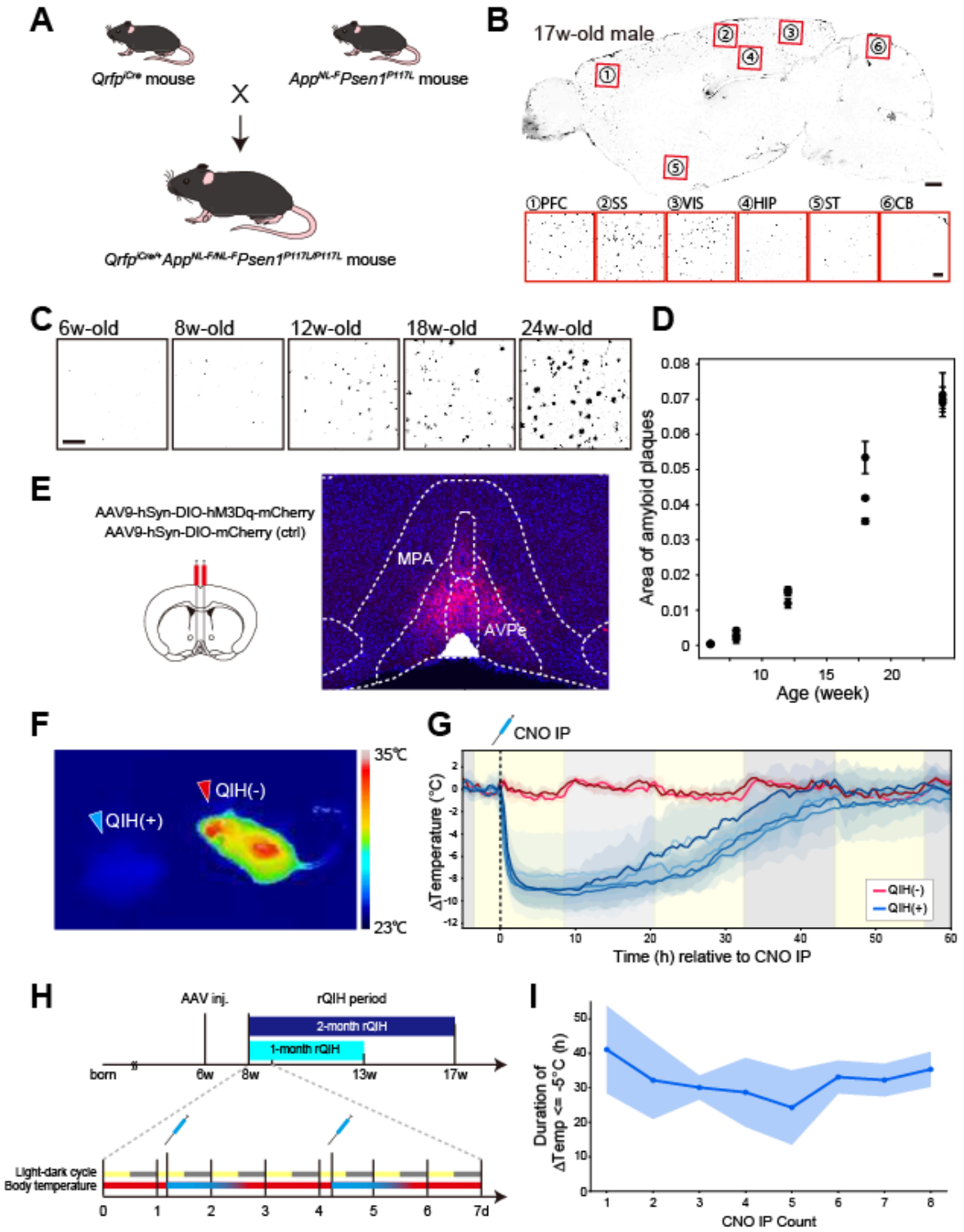

Figure 1: Generation of Q-AD Tg mice and experimental timeline of rQIH

A. Schematic illustration of the generation of Q-AD mice.

B. Sagittal brain image showing Aβ deposition visualized by immunostaining with 82E1 antibody in 17-week-old male Q-AD mice—insets: Enlarged images of the pointed area. Scale bars: 500 μm and 100 μm (inset).

C. Age-dependent progression of amyloid plaque accumulation in the somatosensory cortex in Q-AD male mice. Scale bar: 100 μm.

D. Quantification of Aβ deposition in the motor and somatosensory cortex stained with 82E1 antibody (n = 3 mice for each age).
E. Representative brain image of AAV-injected Q-AD mouse.
AAV9-hSyn-DIO-hM3Dq-mCherry (QIH) or AAV9-hSyn-DIO-mCherry (Ctrl) was injected into the AVPe/MPA.
F. Infrared thermal image of the surface body temperature of CNO-treated Q-AD mice. The image was acquired 3 hours after CNO administration.
G. Temporal progression of hypothermia after DREADD-mediated activation of Q neurons in AAV-injected Q-AD mice.
H. Experimental schema of rQIH. Intraperitoneal (IP) injection of CNO was performed to chemogenetically activate hM3Dq expressed in Q neurons twice a week for 5 or 9 weeks.
I. Quantification of the duration of a 5°C or greater decrease in body temperature due to rQIH (n = 5 mice).

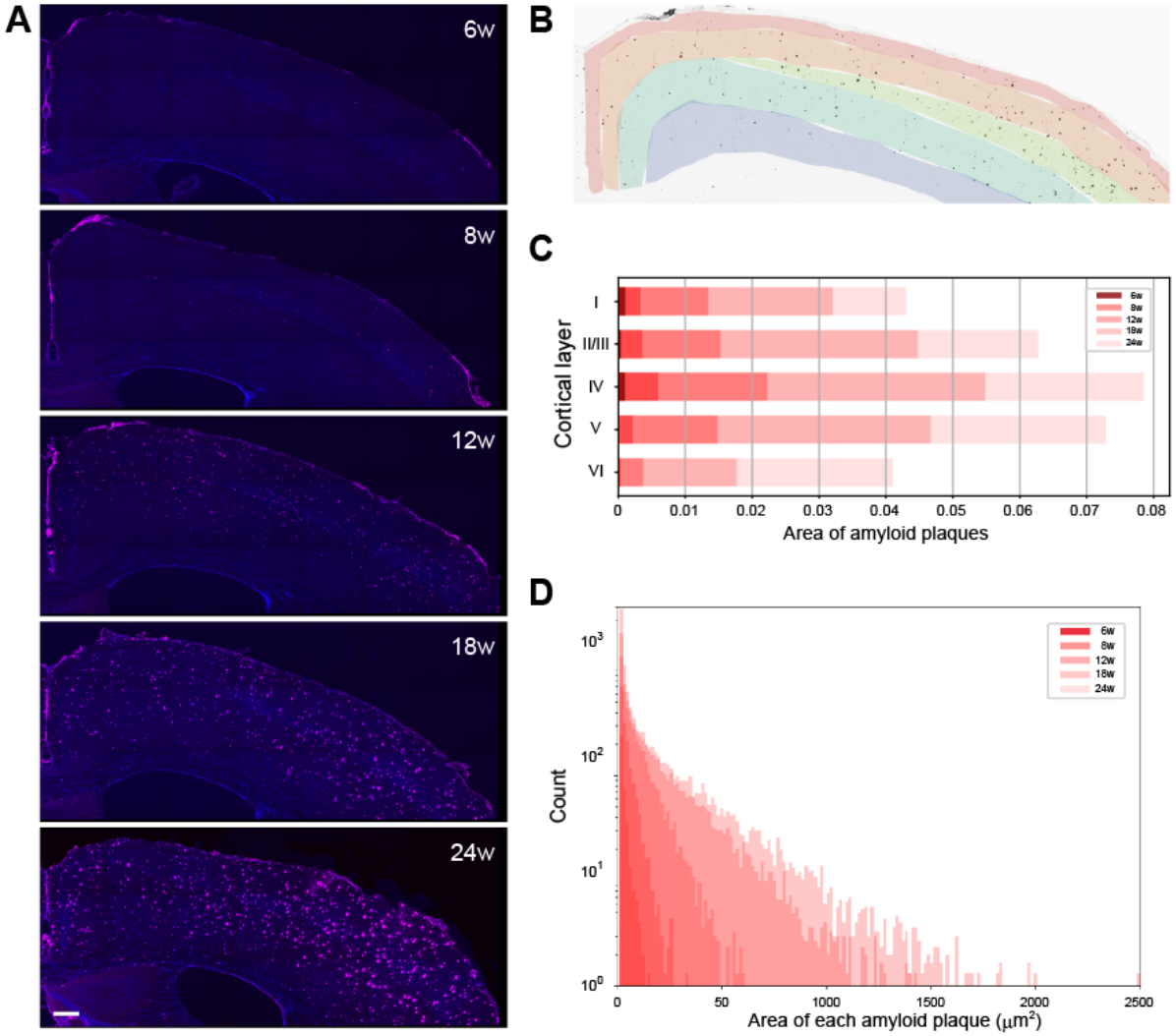

Supplementary Figure 1: Age-dependent progression of amyloid plaque accumulation across cortical layers of male Q-AD mice. (Related to Fig. 1)
A. Representative coronal brain sections showing age-dependent Aβ deposition in 6–24-week-old male Q-AD mice, visualized by immunostaining with 82E1 antibody. Scale

bar: 200 μm.
B. Schematic illustration of cortical layer segmentation used for layer-resolved analysis (L1, L2/3, L4, L5, and L6).
C. Quantification of age-dependent amyloid plaque accumulation in the cerebral cortex of male Q-AD mice. The mean plaque area per animal at each age is shown.
D. Histogram showing the distribution of amyloid plaque sizes at each age. The x-axis represents plaque area (μm²), and the y-axis represents plaque count.

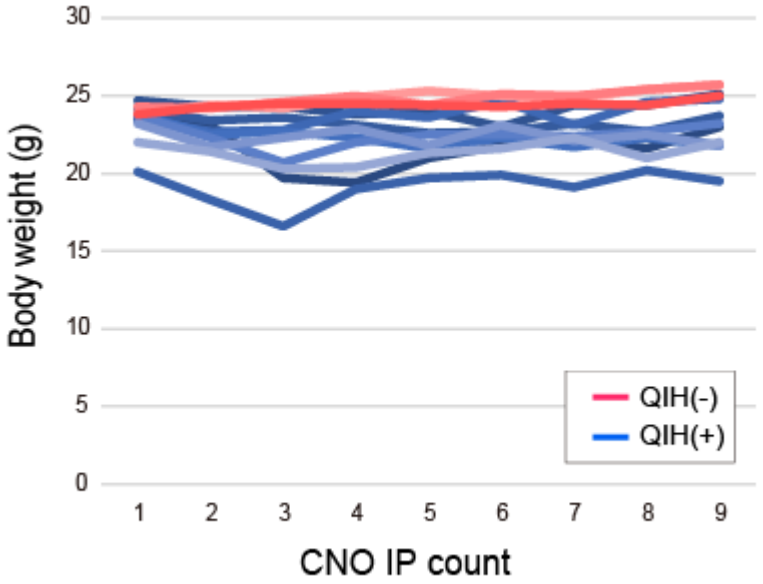

Supplementary Figure 2: Changes in mouse body weight. (Related to Fig. 1)
Some QIH(+) mice showed a slight decrease in their body weight.

rQIH Suppresses Amyloid Plaque Accumulation

We next assessed the effects of rQIH on amyloid pathology in the Q-AD mice. We performed immunohistochemical analyses, which we used previously (Sato et al., 2021; Shimohama et al., 2024), to evaluate amyloid pathology in the brains of 3-month-old Q-AD mice with a 1-month rQIH period (Fig. 2A, B, and C) and 4-month-old Q-AD mice with 2-month rQIH (Fig. 2D, E, and F). The 82E1 antibody, which recognizes the N-terminal epitope of β-secretase–derived Aβ (Iwatsubo et al., 1994), was used to visualize dense amyloid deposits. Compared to QIH(-) control mice in which QIH is not induced because the DREADD receptor was not expressed, we found that amyloid pathology was significantly attenuated by rQIH in the cortex in QIH(+) mice (Fig. 2G and H). The reduction of plaque in the QIH(+) group was greater in the medial regions of the brain, compared to the lateral regions. Interestingly, quantitative analysis of the plaques (see methods in detail) revealed a significant decrease in the number and total area of large (>100 μm²) 82E1-positive amyloid plaques, indicating an overall reduction in Aβ deposition (Fig. 2G, H, and Supplementary Fig. S3). Layer-resolved analyses were performed across the major cortical layers (L1, L2/3, L4, L5, and L6, see methods and Supplementary Fig. 1 in detail). In the 1-month rQIH paradigm,

linear mixed-effects modeling detected modest layer-dependent effects, with relatively larger reductions in Aβ deposition in middle cortical layers, particularly L4 and L5, compared with superficial and deep layers (Supplemental Fig. 4). In contrast, these layer-dependent interactions were no longer evident in the 2-month rQIH group (Supplementary Fig. 4), indicating that prolonged QIH induces a more uniform suppression of amyloid pathology across cortical layers. A significant negative association was observed between plaque area and the average duration of rQIH (Spearman's rank correlation, $\rho = -0.569$, $p = 0.0269$ for 1-month rQIH, and $\rho = -0.777$, $p = 0.0029$ for 2-month rQIH, Fig. 2I). These results indicate that rQIH is associated with a reduction in amyloid pathology in QIH(+) mice.

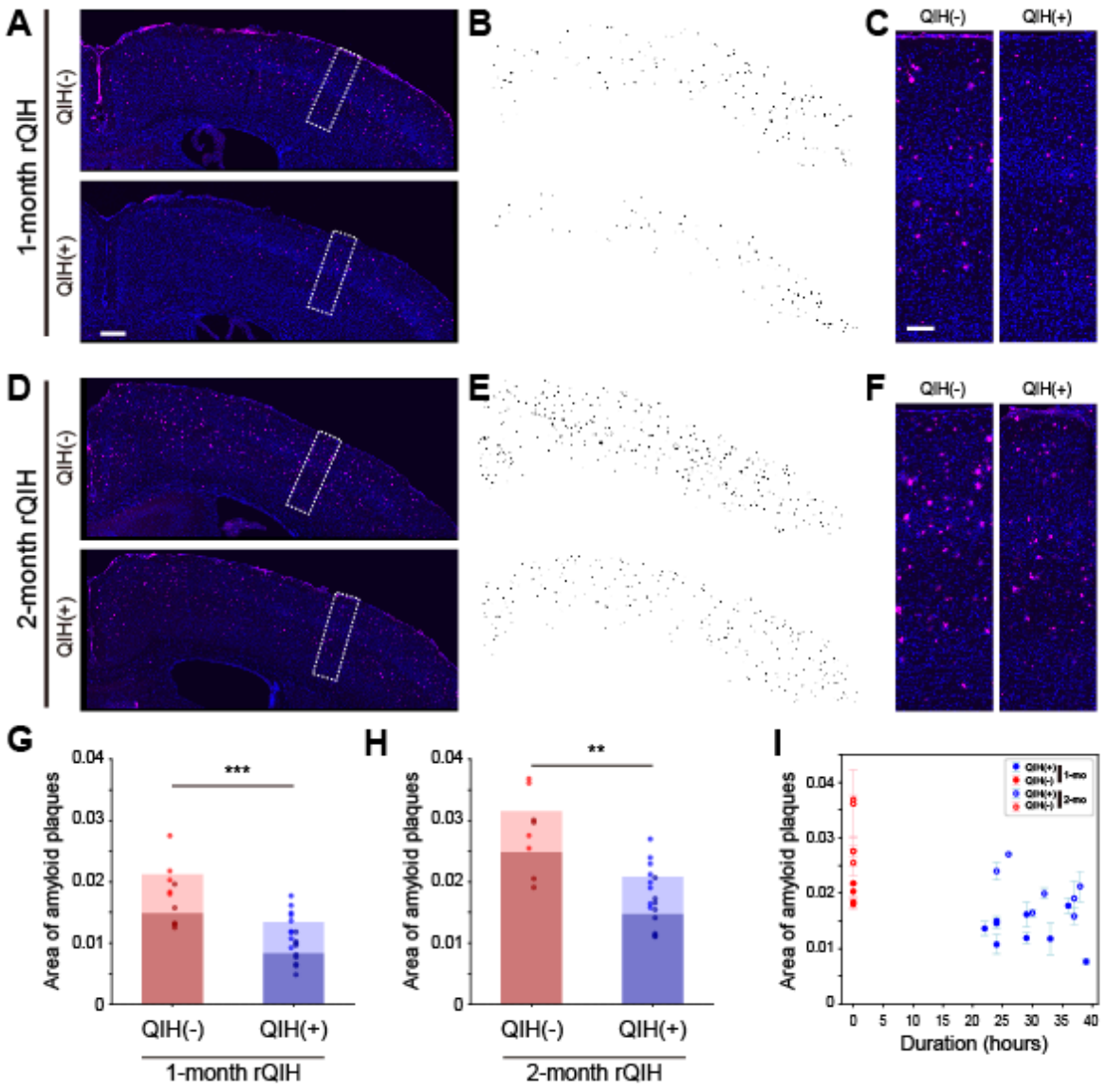

Figure 2: rQIH suppresses the progression of amyloid pathology.
A, D. Representative coronal brain images showing Aβ deposition visualized by immunostaining with 82E1 antibody in 1-month (A) or 2-month (D) rQIH conducted mice. Scale bar, 200 μm.
B, E. Binalized images of Aβ deposition for 1-month (B) or 2-month (E) rQIH. Plaques larger than 100 μm² are visualized.

C, F. Enlarged images of the white-dashed squares in panel A or D. Scale bar, 50 μm.
G, H. Quantification of Aβ deposition in male Q-AD mice subjected to 1-month rQIH (G; QIH(+), n=9; QIH(-), n=5) or 2-month rQIH (H; QIH(+), n=7; QIH(-), n=4). Dark-colored bars indicate quantification of large plaques (>100 μm²). For panel G, p = 0.000666 for plaques ≥10 μm² and p = 0.000666 for plaques ≥100 μm². For panel H, p = 0.008081 for plaques ≥10 μm² and p = 0.01616 for plaques ≥100 μm² (Mann–Whitney U test).
I. Scatter plot showing the relationship between QIH duration and mean plaque area in the cortex. Each marker represents an individual mouse; vertical bars indicate mean ± SD. QIH(-) mice were plotted at duration = 0.

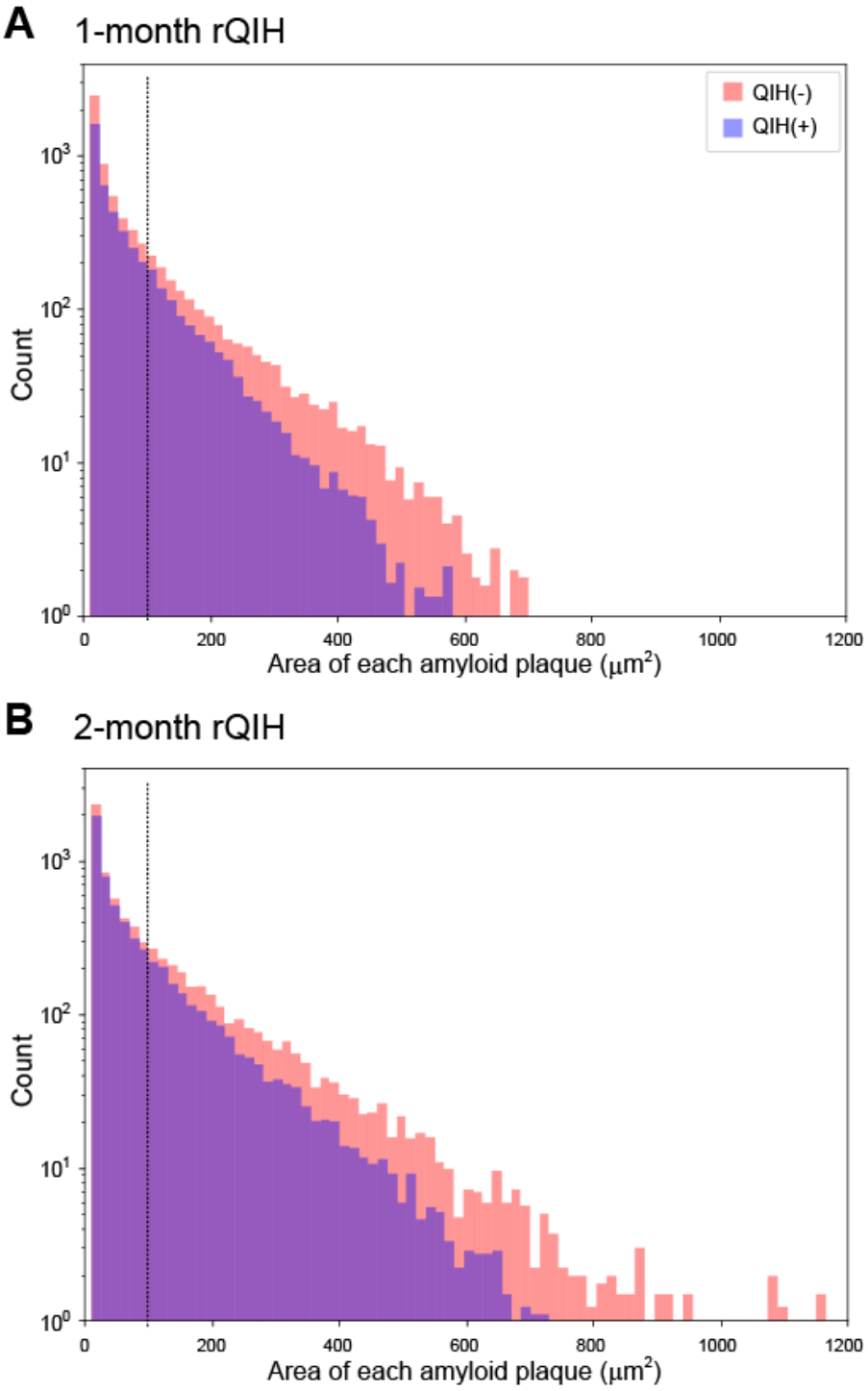

Supplementary Figure 3: Quantification of the effect of rQIH on amyloid pathology. (Related to Fig. 2)
Histogram showing plaque counts as a function of plaque area (A: 1-month rQIH, B: 2-month rQIH). The black dashed line indicates an area of 100μm². Plaque counts for small plaques were comparable between QIH(+) and QIH(−) groups, whereas the number of large plaques (>100 μm²) was markedly reduced in the QIH(+) group.

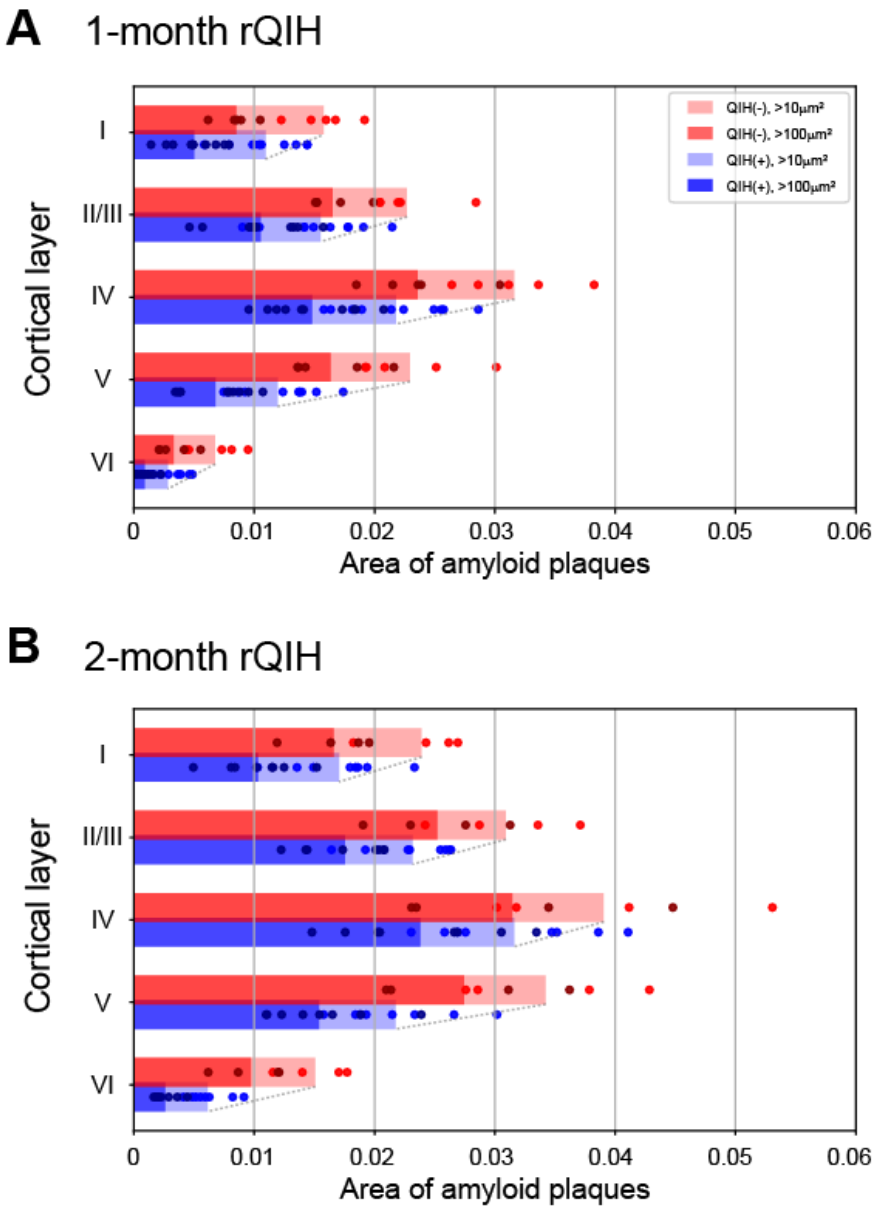

Supplementary Figure 4: Layer-resolved quantification of Aβ deposition in male Q-AD mice subjected to 1-month (A) rQIH or 2-month (B) rQIH. (Related to Fig. 2)
Data are shown as mean values across individual mice. Statistical analysis was performed using a linear mixed-effects model with Condition (QIH(−) vs QIH(+)) and Layer (L1–L6) as fixed effects and mouse identity as a random effect. In the 1-month rQIH group, a significant main effect of Condition was detected ($p = 0.006$), along with a modest but significant Condition × Layer interaction ($p < 0.05$), indicating layer-dependent differences in the magnitude of Aβ reduction. In contrast, in the 2-month rQIH group, although a significant

main effect of Condition was observed ($p = 0.019$), no significant Condition × Layer interaction was detected ($p > 0.05$), indicating a layer-nonspecific reduction of Aβ across the cortex. Thin gray lines connecting QIH(−) and QIH(+) bars indicate the direction and relative magnitude of group differences across layers.

Effects of rQIH on inflammations and neuritic alterations

As amyloid pathology progresses, additional cellular and neuritic alterations accompany plaque formation (Duyckaerts et al., 2009; Selkoe, 2002). We therefore examined whether rQIH-induced changes in amyloid burden were associated with modifications in these downstream features. Neuroinflammation is driven by the activation of microglia and astrocytes and is frequently observed in the brains of patients with AD and in AD model mice, along with preceding amyloid pathology (Heneka et al., 2025; Singh, 2022). We investigated morphological changes in Iba1-positive microglia adjacent to 82E1-positive signals in Q-AD mice. In both the QIH(+) and QIH(-) groups, morphological changes in microglia were observed near plaques, indicating neuroinflammation following Aβ pathology (Supplementary Fig. 5). Despite clear differences in Aβ pathology detected by 82E1 immunostaining, Iba1 immunoreactivity appeared comparable between QIH(+) and QIH(-) groups. This likely reflects a high baseline level of Iba1 expression in microglia during young age, making quantification of differences difficult. In addition to neuroinflammatory responses, neuritic alterations represent another hallmark that emerges during amyloid plaque progression (Tsering & Prokop, 2024). To examine whether rQIH influences plaque-associated neurite pathology, we evaluated dystrophic neurite (DN) formation by co-immunostaining with antibodies against 82E1 and Lamp1 (Fig. 3A and B). Lamp1-positive signals were frequently observed surrounding 82E1-positive amyloid plaques, consistent with plaque-associated neuritic dystrophy. In contrast, smaller Aβ plaques were often not accompanied by detectable Lamp1 signals (Fig. 3B). Quantitative analysis revealed that the total area of Lamp1-labeled DNs was significantly reduced in the 1-month rQIH(+) group compared with rQIH(-) controls (Fig. 3C, $p = 0.0286$). In the 2-month rQIH paradigm, Lampq-positive DN area also tended to be reduced in rQIH(+) mice; however, this difference did not reach statistical significance ($p = 0.0571$; Fig. 3D). Together, these results indicate that while overt microglial activation assessed by Iba1 immunoreactivity was not detectably altered at these early disease stages, rQIH is associated with a reduction in plaque-associated neuritic dystrophy, suggesting an attenuation of secondary neuritic alterations accompanying amyloid plaque progression.

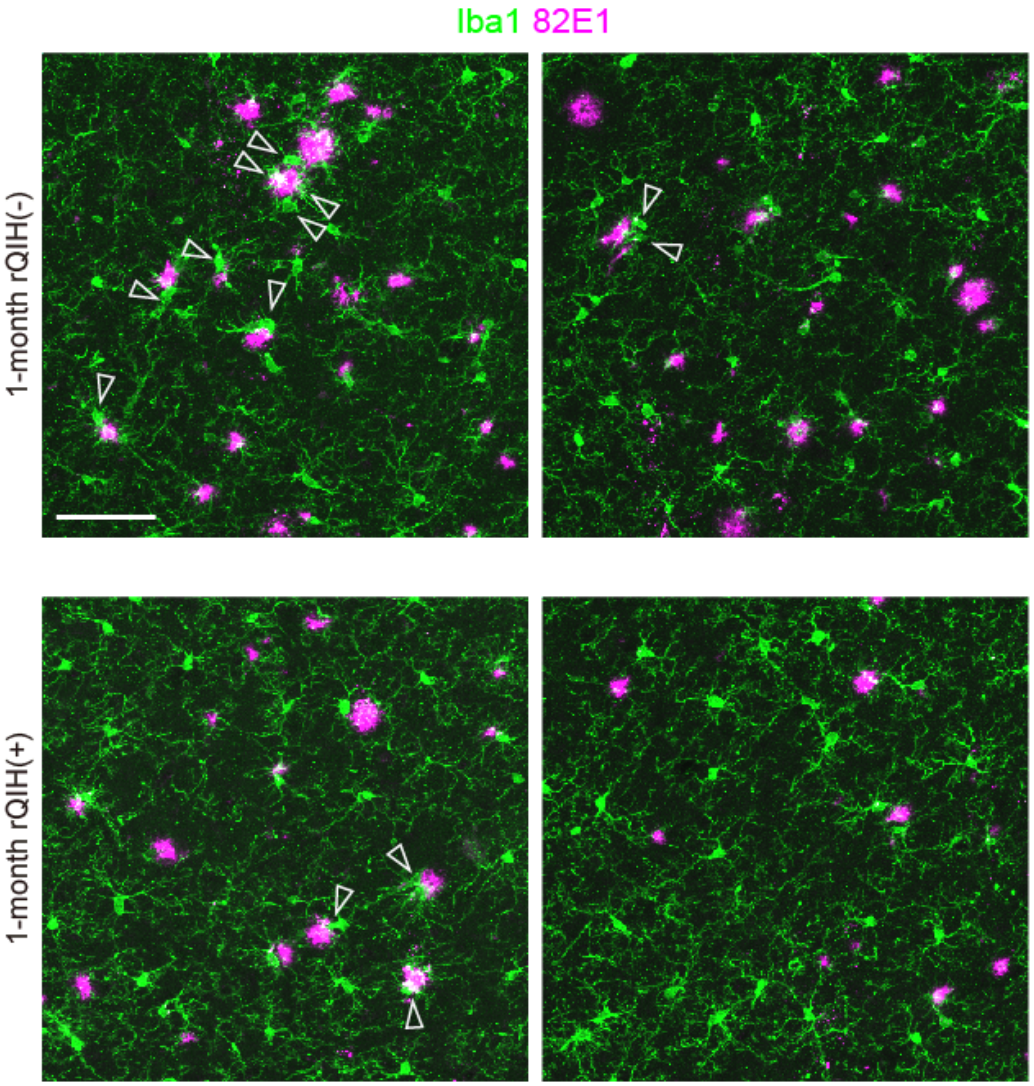

Supplementary Figure 5: Neuroinflammation in Q-AD mice upon rQIH. (Related to Fig. 3)
Coronal brain images showing Aβ deposition and microglia visualized by immunostaining with 82E1 (magenta) and Iba1 (green) antibody. Allowheads indicate the amoeboid-shaped Iba1^{+} microglia. Scale bar, 100 μm.

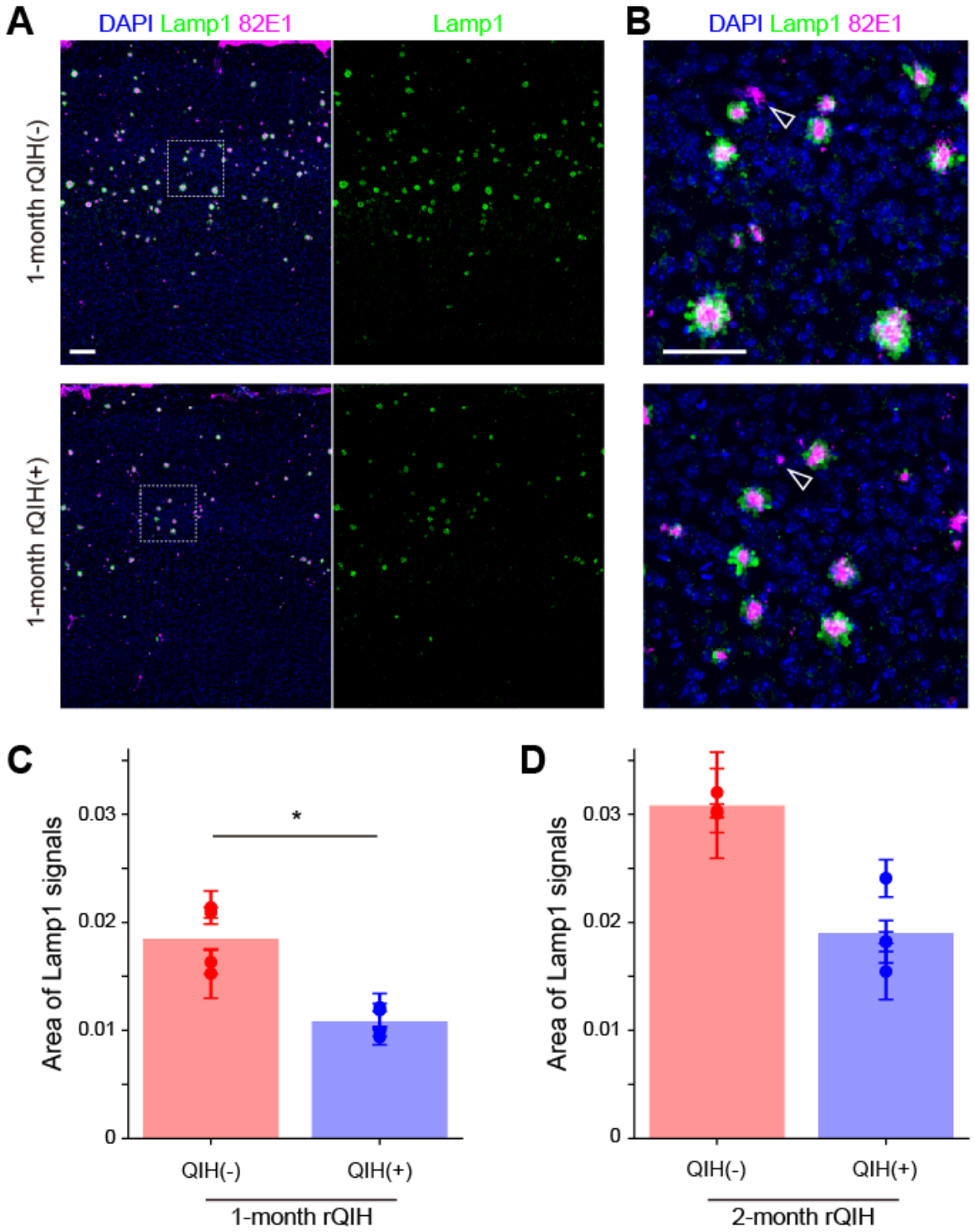

Figure 3: Neuritic alterations in Q-AD mice upon rQIH.
A. Coronal brain image showing Aβ deposition and neuritic alterations visualized by immunostaining with 82E1 (magenta) and Lamp1 (green) antibody. Allowheads indicate the 82E1 signals lacking Lamp1 signals. Scale bar, 100 μm.
B. Enlarged image of the dashed square area in A. Scale bar, 50 μm.
C, D. Quantification of Lamp1 signals in the cortex (n=4 for QIH(+), n=4 for QIH(-) for 1mo-QIH, C, n=4 for QIH(+), n=3 for QIH(-) for 2mo-QIH, C).

Discussion

Summary

In this study, we generated a novel hibernation-like state–inducible AD model mouse by cross-mating an AD model line with hibernation-like state–inducible QrfpiCre mice, thereby enabling induction of Q neuron–induced hibernation-like states (QIH) in an AD background (Fig. 1). Using these animals, we demonstrated that repeated QIH induction (rQIH) suppresses the progression of amyloid pathology (Fig. 2). The suppressive effect was greater when QIH lasted longer, and rQIH specifically reduced large 82E1-positive amyloid plaques (Fig. 2), accompanied by a reduction in dystrophic neurite formation (Fig. 3). We further established a protocol for repetitive induction of QIH by repeated administration of CNO, twice per week for one to two months. Under the experimental conditions tested, this protocol induced a hibernation-like state for prolonged periods without detectable adverse effects on animal health, as assessed by body weight, survival, and general behavioral observations (Fig. 1).

Proof of concept: suppressing amyloid pathology by manipulating a brain-wide physiological state

These findings provide a proof of concept that repeated induction of a hibernation-like state can suppress the progression of early amyloid pathology by manipulating a brain-wide physiological state. Whereas amyloid pathology has most often been discussed within a framework of targeting individual molecular components of amyloid metabolism (Hampel et al., 2021; Mucke & Selkoe, 2012; Zhang et al., 2012), our study was designed not to test a single predefined molecular pathway, but rather to ask whether a hibernation-like, integrated hypometabolic state itself can influence amyloid pathology. Although we do not yet delineate the precise molecular mechanisms underlying this effect, our results demonstrate the feasibility of modulating amyloid pathology by manipulating the global brain metabolic state.

Mechanisms underlying the suppressive effect of QIH on amyloid pathology

Several non-mutually exclusive mechanisms could account for the observed suppression of amyloid progression during QIH. First, QIH-induced hypometabolism may reduce Aβ production and/or release. Hypometabolic states are known to broadly suppress transcriptional and translational processes (Gautier et al., 2018; Storey & Storey, 2010). Thus, QIH may downregulate APP expression and thereby reduce the supply of its cleavage product, amyloid-β (Aβ), attenuating initiation and progression of amyloid pathology. Consistent with this idea, modest down-regulation of APP expression in transgenic mouse models decreases soluble and insoluble Aβ levels and reduces amyloid plaque burden (Asuni et al., 2014). In addition, metabolic depression may reduce neuronal activity, and if extracellular Aβ release is activity-dependent, reduced activity could decrease synaptic Aβ release and slow amyloid progression (Cirrito et al., 2005, 2008). This interpretation is also consistent with reports that global metabolic downregulation, such as caloric restriction, attenuates Aβ generation and amyloid plaque deposition in AD model mice (J. Wang et al., 2005).

Second, QIH may enhance extracellular Aβ clearance. The glymphatic system is highly active during sleep and facilitates the removal of extracellular metabolites, including Aβ (Silva et al., 2021; Xie et al., 2013). Moreover, accumulating evidence indicates that sleep and circadian changes are not merely secondary to neurodegeneration but can actively

regulate neurodegenerative processes, including Aβ metabolism (Musiek & Holtzman, 2016). If the QIH-induced state engages sleep-like pathways—through reduced metabolism, altered perfusion, or changes in fluid dynamics—the reduction in Aβ burden observed here could reflect, at least in part, enhanced clearance rather than solely decreased production.
Third, QIH may dampen neuroinflammation, potentially mitigating immune-mediated amplification of AD pathology. In Alzheimer's disease, chronic microglial activation, complement dysregulation, and broader immune-driven neuroinflammation are widely implicated in amplifying pathology and neurodegeneration (Heneka et al., 2015, 2025; Hong et al., 2016; Leng & Edison, 2021). In natural hibernators, peripheral immune cell numbers and immune responses are reduced in a reversible manner (Bouma et al., 2013; Sahdo et al., 2013). In addition, hibernation is associated with changes in microglial morphology and distribution in the CNS and may shift the brain toward a less inflammatory state (León-Espinosa et al., 2018; Zhou et al., 2001). Thus, rQIH might attenuate immune-dependent neuronal injury around Aβ deposits, contributing to the observed reduction in dystrophic neurite formation.
Fourth, environmental cold exposure during the QIH protocol may contribute to the observed effects. However, the contribution of temperature per se is difficult to interpret, because ambient cooling can increase metabolic demand as mammals attempt to maintain body temperature (Muñoz Zamora et al., 2025). Notably, mild or chronic exposure to environmental cold has been reported not to significantly alter Aβ or tau pathology (McFadden et al., 2023), suggesting that reduced ambient temperature per se may be insufficient to robustly modulate amyloid-related processes. Based on the above considerations for the fourth possibility, the suppressive effect observed here is unlikely to be explained by environmental cold exposure per se (i.e., a decrease in ambient temperature) alone. Rather, it is more likely that one or more of the mechanisms proposed above (1–3) acted in combination, potentially synergistically, within the coordinated hypometabolic/hypothermic state induced by QIH.

Physiological and therapeutic implications

The suppressive effect on amyloid progression observed here can be interpreted as a slowing, or temporary arrest, of pathological advancement. Such an effect could preserve a therapeutic time window, thereby enabling subsequent and potentially more interventional treatment strategies. Importantly, our approach leverages endogenous physiological mechanisms rather than directly targeting pathology through a single pharmacological pathway. If QIH influences amyloid pathology in part by enhancing clearance of extracellular metabolites, similar clearance-associated benefits may extend to other age-related neurodegenerative diseases (Iliff et al., 2012; Rasmussen et al., 2018). More broadly, inducing a controlled hypometabolic brain state, or mimicking key molecular features of hibernation, may represent a promising avenue for disease-modifying strategies in preclinical or early-stage AD.

Limitations and future directions

This proof-of-concept study has several limitations. First, our analyses focused on early-stage amyloid pathology; the long-term effects following rQIH, the impact of later-stage rQIH, and effects on cognitive function remain unexplored. Second, while we primarily examined Aβ pathology, other major disease axes, including tau pathology, were not

investigated. Third, because our results are based on transgenic-derived APP overexpression, we cannot determine the extent to which rQIH affects APP production at more intrinsic levels. In addition, the double-mutant model used here exhibits extremely rapid progression and a severe phenotype; studies in milder models may reveal larger effects, potentially extending beyond suppressing progression to producing measurable improvement.

A key open question is which processes—reduced Aβ production/release, enhanced extracellular clearance, and/or immune modulation—are necessary and sufficient for the suppressive effect observed during QIH. Disentangling these contributions will require direct measurements of soluble and insoluble Aβ species, analyses of APP processing pathways (e.g., western blot, proteome analysis), and tests of clearance mechanisms (including glymphatic function), along with profiling of neuroinflammatory and immune-related responses.

Another important issue is whether the suppressive effect arises primarily from hypothermia or metabolic suppression. Prior work shows that manipulating thermoregulatory circuits can induce metabolic suppression and torpor-like states even under warm ambient conditions (Lee et al., 2025). Such approaches could help test the effect of metabolic suppression while minimizing hypothermia, thereby clarifying their relative contributions. Conversely, because our mice were maintained at room temperature, the reduction in body temperature was limited to room-temperature levels; deeper hypothermia—more typical of natural hibernation—might be achieved by maintaining animals in a cold room during QIH, potentially enhancing suppression.

Conclusion

Together, our findings demonstrate that manipulating a hibernation-like, integrated hypometabolic brain state can modulate early amyloid pathology. QIH provides a tractable experimental framework for probing brain-state–dependent metabolism–pathology interactions in Alzheimer's disease and for identifying physiological levers that may influence disease progression.

Resource availability

Lead contact

Further information and requests for resources and reagents should be directed to the Lead Contact, Masanori Murayama (masanori.murayama@riken.jp), who will fulfill them.

Materials availability

Materials generated in this study are available from the corresponding author upon reasonable request.

Data and code availability

The data supporting the findings of this study and the custom code used for data analysis are available from the corresponding author upon reasonable request.

Acknowledgments

We thank J. Nagai, and all lab members for comments and discussions on the project; the Support Unit for Bio-Material Analysis, RIKEN CBS Research Resources Division, and especially R. Ando for technical assistance with AAV injections, A. Ito for technical assistance with embryo manipulation; and Y. Mizukami, N. Kaieda, and K. Ueno for animal care. This project was supported by the Japan Society for the Promotion of Science (JSPS) Grant-in-Aid for Transformative Research Areas (A) (JP23H04941 to G.A.S.); JSPS KAKENHI Grant-in-Aid for Scientific Research (C) (JP18K07402 to H.S.); JSPS KAKENHI (JP24H02313 to M.M.); the Japan Science and Technology Agency (JST) FOREST Program (JPMJFR2066 to G.A.S.); and the Japan Agency for Medical Research and Development (AMED) Brain/MINDS 2.0 Project (JP23wm0625001 to H.S and M.M.).

Author contributions

I.O., H.S., G.A.S., and M. M. conceptualized the project. I.O., H.Y., and M.O. conducted the experiments. I.O. analyzed the data. H.S., G.A.S., and M. M. supervised the project. H.S., G.A.S., T.S., and M. M. had a general discussion on the project. I.O., H.Y., G.A.S., and M. M. wrote the manuscript.

Declaration of interests

The authors declare no competing interests.

Declaration of generative AI and AI-assisted technologies

During the preparation of this work, the authors used ChatGPT and Grammarly in order to improve language and readability. After using these tools, the authors reviewed and edited the content as needed and take full responsibility for the content of the publication.

Materials and Methods

Animals

All animal experiments were performed in accordance with the institutional guidelines and were approved by the Animal Experiment Committee at RIKEN. Double-mutant AD model mice (App/Psen1; (Sato et al., 2021)) and Qrfp^{iCre} mice (Takahashi et al., 2020) were used. The triple transgenic Q-AD mouse was generated by crossing App/Psen1 mice with Qrfp mice or through embryonic manipulation. Both male and female mice aged 6-24 weeks and weighing over 16.0 g for males and 15.0 g for females at 6 weeks old were used in the study without disparity. Mice were housed under controlled conditions (22-24 °C, 40-60% humidity, 12 h light/12 h dark light cycle) with ad libitum access to food and water.

Viruses

Adeno-associated viruses (AAV) were purchased from Addgene: AAV9-hSyn-DIO-hM3D(Gq)-mCherry (44361-AAV9) and AAV9-hSyn-DIO-mCherry (50459-AAV9).

Surgery

For AAV vector injection, 6-week-old mice were anaesthetized with isoflurane (2%) for induction. Once the mice failed to respond to stimuli, we administered a hypodermic injection of the combination agent (Kawai2011-fq) – Medetomidine/Midazolam/Butorphanol (MMB) – at a dose of 5 mL/kg body weight for the procedure. We dispensed MMB solution with medetomidine (0.12 mg/kg body weight), midazolam (0.32 mg/kg body weight), butorphanol (0.4 mg/kg body weight), and saline. After anesthesia with MMB, the head hair of the mice was shaved, and they were placed in head holders (SG-4N, NARISHIGE). During surgery, the mice's body temperature was maintained at 36–37 °C using a feedback-controlled heat pad (BWT-100, Bio Research Center), and their eyes were coated with ointment (Neo-Medrol EE Ointment, Pfizer Inc.). The scalp was cleaned with 70% ethanol and iodine, and then incised to expose the skull surface. Mice underwent injection of AAV9-hSyn-DIO-hM3Dq-mCherry or AAV9-hSyn-DIO-mCherry into the AVPe/MPA: anterior–posterior (AP), +0.83 mm; medial–lateral (ML), ± 0.3 mm; dorsal–ventral (DV), −5.25 mm; 0.1 μl in each site at a controlled rate of 0.1 μl per 10 min using a pulled fine-glass capillary. The needle was kept in place for 10 min before and after the injection. After the surgery, the mice were dispensed a medetomidine-reversing agent, atipamezole hydrochloride (ANTISEDAN, zoetis Inc.) solution at a dose of 0.12 mg/kg body weight, then the mice were recovered on a heating pad. The waiting period for recovery and virus expression for the experiments was 2 weeks.

For the implantation of a small motion measurement device (nano tag; KISSEI COMTEC), mice were anaesthetized with isoflurane (2%) for induction, followed by MMB. The hair on the back was shaved, and the skin was cleaned with 70% ethanol and iodine. After making a vertical incision approximately 1.5 cm in length in the skin, the nanotag was inserted, and the skin was sutured with nylon thread (ER2004NA45-KF2, alfresa). The suture site was bonded using the medical adhesive derma+flex (CHEMENCE) to maintain joint strength. After the surgery, the mice were dispensed atipamezole hydrochloride.

Chemogenetic induction of QIH

CNO (BML-NS105-0025, Enzo) was dissolved in saline at a dose of 1mg ml^{-1} and frozen at −20 °C. The CNO solution was thawed, diluted 10-fold with saline (100 μg ml^{-1}), and administered intraperitoneally at a dose of 1 mg kg−1 to mice.

Body temperature and locomotion recordings

Body temperature and locomotor activity were monitored at 5-minute intervals using an implanted nano tag. The acquired data were imported into the accompanying software (nanotag Viewer, KISSEI COMTEC) and analyzed using custom Python scripts.

For thermographic analysis, mice were placed in experimental cages (28.5 × 17.5 × 12.5 cm) and imaged with an infrared thermal camera (Mini2 V2, HIKMICRO) mounted on an iPhone 13 mini (Apple), positioned 30 cm above the cage floor.

Immunohistochemistry, imaging, and analysis

The mice were deeply anesthetized by intraperitoneal injection of MMB and perfused transcardially with PBS supplemented with heparin (10 units/mL), followed by 4% paraformaldehyde (PFA) in phosphate-buffer saline (PBS; pH 7.4). The brains were then harvested and post-fixated in PFA overnight at 4 °C. The brains were cryoprotected with 30% sucrose in PBS and sectioned into 40-μm-thick coronal or sagittal sections using a freezing microtome (ROM-380, Yamato).

For immunohistochemistry, the sections were incubated in a blocking solution (2% normal goat serum and 0.3% TritonX-100 in PBS) for 30 min at room temperature. The sections were then incubated in a blocking solution containing a primary antibody, overnight at 4 °C, and subsequently washed three times with a washing buffer (0.3% TritonX-100 in PBS). The sections were incubated in a blocking solution containing a secondary antibody conjugated to a fluorescent dye for 2 h at room temperature, then washed three times with the washing buffer. The sections were stained for 15 min with DAPI (D9542, sigma) diluted in PBS and then mounted onto slides using a Fluoromount/Plus anti-fading agent (K048; Diagnostic BioSystems). Section images were obtained using a confocal laser-scanning microscope (FV-3000, Evident). Quantification of immunofluorescent signals was performed using ImageJ software.

Primary and secondary antibodies used in this study are as follows: anti-Iba1 (WAKO, 019-19741), anti-human amyloid β (N; 82E1; IBL, #10323), anti-LAMP1 (Abcam, ab208943), Goat anti-Mouse IgG (H+L) Highly Cross-Adsorbed Secondary Antibody, Alexa Fluor Plus 647 (Thermo, A32728), and Goat anti-Rabbit IgG (H+L) Highly Cross-Adsorbed Secondary Antibody, Alexa Fluor Plus 488 (Thermo, A32731).

Quantification and statistical analysis

Image quantification was performed using ImageJ/Fiji (NIH). For amyloid plaque size quantification, immunofluorescence images of 82E1-stained coronal brain sections were binarized using the MaxEntropy thresholding method, applied consistently across samples within each experiment. To minimize the inclusion of noise and non-specific signals, particles smaller than 10 μm² were excluded from all analyses. Plaque-related analyses were conducted on particles ≥10 μm², and analyses focusing on large plaques applied an additional threshold of ≥100 μm². For dystrophic neurite quantification, Lamp1 immunofluorescence images of coronal brain sections were first subjected to background subtraction using a rolling ball radius of 50 pixels, followed by binarization using the Moments thresholding method, applied consistently across samples within each experiment. To further reduce noise and non-specific signals, particles smaller than 50 μm² were excluded from all analyses.

Quantification was performed in two ways: (i) across the entire cortical region and (ii) separately within individual cortical layers (L1, L2/3, L4, L5, and L6). Cortical layers were

manually defined as regions of interest (ROIs) based on DAPI nuclear staining as anatomical landmarks.

For whole-cortex quantification, statistical comparisons between control (QIH(-)) and QIH(+) groups were performed using the Mann–Whitney U test. Correlations between QIH duration and plaque size were assessed using Spearman's rank correlation coefficient.

Layer-resolved analyses were performed using a linear mixed-effects model (LMM). Condition (QIH(-) vs QIH(+)), Layer (L1–L6), and their interaction were treated as fixed effects, while mouse identity was included as a random effect to account for repeated measurements across cortical layers within the same animal.

All statistical analyses were performed using Python (v3.7.11), primarily utilizing the statsmodels and SciPy libraries. Data are presented as mean ± SD unless otherwise specified. Exact p-values are reported in the figures or figure legends. Statistical significance was defined as $p < 0.05$.

Supplemental information

References

Asuni, A. A., Guridi, M., Pankiewicz, J. E., Sanchez, S., & Sadowski, M. J. (2014). Modulation of amyloid precursor protein expression reduces β-amyloid deposition in a mouse model. *Annals of Neurology*, *75*(5), 684–699. https://doi.org/10.1002/ana.24149

Bouma, H. R., Henning, R. H., Kroese, F. G. M., & Carey, H. V. (2013). Hibernation is associated with depression of T-cell independent humoral immune responses in the 13-lined ground squirrel. *Developmental & Comparative Immunology*, *39*(3), 154–160. https://doi.org/10.1016/j.dci.2012.11.004

CAREY, H. V., ANDREWS, M. T., & MARTIN, S. L. (2003). Mammalian Hibernation: Cellular and Molecular Responses to Depressed Metabolism and Low Temperature. *Physiological Reviews*, *83*(4), 1153–1181. https://doi.org/10.1152/physrev.00008.2003

Cirrito, J. R., Kang, J.-E., Lee, J., Stewart, F. R., Verges, D. K., Silverio, L. M., Bu, G., Mennerick, S., & Holtzman, D. M. (2008). Endocytosis Is Required for Synaptic

Activity-Dependent Release of Amyloid-β In Vivo. *Neuron*, *58*(1), 42–51. https://doi.org/10.1016/j.neuron.2008.02.003

Cirrito, J. R., Yamada, K. A., Finn, M. B., Sloviter, R. S., Bales, K. R., May, P. C., Schoepp, D. D., Paul, S. M., Mennerick, S., & Holtzman, D. M. (2005). Synaptic Activity Regulates Interstitial Fluid Amyloid-β Levels In Vivo. *Neuron*, *48*(6), 913–922. https://doi.org/10.1016/j.neuron.2005.10.028

Dave, K. R., Christian, S. L., Perez-Pinzon, M. A., & Drew, K. L. (2012). Neuroprotection: Lessons from hibernators. *Comparative Biochemistry and Physiology Part B: Biochemistry and Molecular Biology*, *162*(1), 1–9. https://doi.org/10.1016/j.cbpb.2012.01.008

Duyckaerts, C., Delatour, B., & Potier, M.-C. (2009). Classification and basic pathology of Alzheimer disease. *Acta Neuropathologica*, *118*(1), 5–36. https://doi.org/10.1007/s00401-009-0532-1

Frisoni, G. B., Altomare, D., Thal, D. R., Ribaldi, F., van der Kant, R., Ossenkoppele, R., Blennow, K., Cummings, J., van Duijn, C., Nilsson, P. M., Dietrich, P.-Y., Scheltens, P., & Dubois, B. (2022). The probabilistic model of Alzheimer disease: The amyloid hypothesis revised. *Nature Reviews Neuroscience*, *23*(1), 53–66. https://doi.org/10.1038/s41583-021-00533-w

Gautier, C., Bothorel, B., Ciocca, D., Valour, D., Gaudeau, A., Dupré, C., Lizzo, G., Brasseur, C., Riest-Fery, I., Stephan, J.-P., Nosjean, O., Boutin, J. A., Guénin, S.-P., & Simonneaux, V. (2018). Gene expression profiling during hibernation in the European hamster. *Scientific Reports*, *8*(1), 13167. https://doi.org/10.1038/s41598-018-31506-2

Hampel, H., Hardy, J., Blennow, K., Chen, C., Perry, G., Kim, S. H., Villemagne, V. L., Aisen, P., Vendruscolo, M., Iwatsubo, T., Masters, C. L., Cho, M., Lannfelt, L., Cummings, J. L., & Vergallo, A. (2021). The Amyloid-β Pathway in Alzheimer's Disease. *Molecular Psychiatry*, *26*(10), 5481–5503. https://doi.org/10.1038/s41380-021-01249-0

Heneka, M. T., Carson, M. J., Khoury, J. E., Landreth, G. E., Brosseron, F., Feinstein, D. L., Jacobs, A. H., Wyss-Coray, T., Vitorica, J., Ransohoff, R. M., Herrup, K., Frautschy,

S. A., Finsen, B., Brown, G. C., Verkhratsky, A., Yamanaka, K., Koistinaho, J., Latz, E., Halle, A., … Kummer, M. P. (2015). Neuroinflammation in Alzheimer's disease. *The Lancet Neurology*, *14*(4), 388–405. https://doi.org/10.1016/S1474-4422(15)70016-5

Heneka, M. T., van der Flier, W. M., Jessen, F., Hoozemanns, J., Thal, D. R., Boche, D., Brosseron, F., Teunissen, C., Zetterberg, H., Jacobs, A. H., Edison, P., Ramirez, A., Cruchaga, C., Lambert, J.-C., Laza, A. R., Sanchez-Mut, J. V., Fischer, A., Castro-Gomez, S., Stein, T. D., … Riechers, S.-P. (2025). Neuroinflammation in Alzheimer disease. *Nature Reviews Immunology*, *25*(5), 321–352. https://doi.org/10.1038/s41577-024-01104-7

Hong, S., Beja-Glasser, V. F., Nfonoyim, B. M., Frouin, A., Li, S., Ramakrishnan, S., Merry, K. M., Shi, Q., Rosenthal, A., Barres, B. A., Lemere, C. A., Selkoe, D. J., & Stevens, B. (2016). Complement and microglia mediate early synapse loss in Alzheimer mouse models. *Science*, *352*(6286), 712–716. https://doi.org/10.1126/science.aad8373

Iliff, J. J., Wang, M., Liao, Y., Plogg, B. A., Peng, W., Gundersen, G. A., Benveniste, H., Vates, G. E., Deane, R., Goldman, S. A., Nagelhus, E. A., & Nedergaard, M. (2012). A Paravascular Pathway Facilitates CSF Flow Through the Brain Parenchyma and the Clearance of Interstitial Solutes, Including Amyloid β. *Science Translational Medicine*, *4*(147), 147ra111-147ra111. https://doi.org/10.1126/scitranslmed.3003748

Iwatsubo, T., Odaka, A., Suzuki, N., Mizusawa, H., Nukina, N., & Ihara, Y. (1994). Visualization of Aβ42(43) and Aβ40 in senile plaques with end-specific Aβ monoclonals: Evidence that an initially deposited species is Aβ42(43). *Neuron*, *13*(1), 45–53. https://doi.org/10.1016/0896-6273(94)90458-8

Jack, C. R., Knopman, D. S., Jagust, W. J., Shaw, L. M., Aisen, P. S., Weiner, M. W., Petersen, R. C., & Trojanowski, J. Q. (2010). Hypothetical model of dynamic biomarkers of the Alzheimer's pathological cascade. *The Lancet Neurology*, *9*(1), 119–128. https://doi.org/10.1016/S1474-4422(09)70299-6

Lee, M.-L., Chang, C.-P., Toda, C., Nemoto, T., & Enoki, R. (2025). Body temperature regulates glucose metabolism and torpid behavior. *Nature Communications*, *16*(1), 6278. https://doi.org/10.1038/s41467-025-61499-2

Leng, F., & Edison, P. (2021). Neuroinflammation and microglial activation in Alzheimer disease: Where do we go from here? *Nature Reviews Neurology*, *17*(3), 157–172. https://doi.org/10.1038/s41582-020-00435-y

León-Espinosa, G., Regalado-Reyes, M., DeFelipe, J., & Muñoz, A. (2018). Changes in neocortical and hippocampal microglial cells during hibernation. *Brain Structure and Function*, *223*(4), 1881–1895. https://doi.org/10.1007/s00429-017-1596-7

McFadden, S., Sime, L. N., Cox, M. F., Findley, C. A., Peck, M. R., Quinn, K., Fang, Y., Bartke, A., Hascup, E. R., & Hascup, K. N. (2023). Chronic, Mild Hypothermic Environmental Temperature Does Not Ameliorate Cognitive Deficits in an Alzheimer's Disease Mouse. *The Journals of Gerontology: Series A*, *78*(6), 911–919. https://doi.org/10.1093/gerona/glac223

Mucke, L., & Selkoe, D. J. (2012). Neurotoxicity of Amyloid β-Protein: Synaptic and Network Dysfunction. *Cold Spring Harbor Perspectives in Medicine*, *2*(7), a006338. https://doi.org/10.1101/cshperspect.a006338

Muñoz Zamora, A., Douglas, A., Conway, P. B., Urrieta, E., Moniz, T., O'Leary, J. D., Marks, L., Denny, C. A., Ortega-de San Luis, C., Lynch, L., & Ryan, T. J. (2025). Cold memories control whole-body thermoregulatory responses. *Nature*, *641*(8064), 942–951. https://doi.org/10.1038/s41586-025-08902-6

Musiek, E. S., & Holtzman, D. M. (2016). Mechanisms linking circadian clocks, sleep, and neurodegeneration. *Science*, *354*(6315), 1004–1008. https://doi.org/10.1126/science.aah4968

Oh, H., Madison, C., Baker, S., Rabinovici, G., & Jagust, W. (2016). Dynamic relationships between age, amyloid-β deposition, and glucose metabolism link to the regional vulnerability to Alzheimer's disease. *Brain*, *139*(8), 2275–2289. https://doi.org/10.1093/brain/aww108

Rafii, M. S., & Aisen, P. S. (2023). Detection and treatment of Alzheimer's disease in its preclinical stage. *Nature Aging*, *3*(5), 520–531. https://doi.org/10.1038/s43587-023-00410-4

Rasmussen, M. K., Mestre, H., & Nedergaard, M. (2018). The glymphatic pathway in neurological disorders. *The Lancet Neurology*, *17*(11), 1016–1024. https://doi.org/10.1016/S1474-4422(18)30318-1

Sahdo, B., Evans, A. L., Arnemo, J. M., Fröbert, O., Särndahl, E., & Blanc, S. (2013). Body Temperature during Hibernation Is Highly Correlated with a Decrease in Circulating Innate Immune Cells in the Brown Bear (*Ursus arctos*): A Common Feature among Hibernators? *International Journal of Medical Sciences*, *10*(5), 508–514. https://doi.org/10.7150/ijms.4476

Sakurai, L., Yoshimoto, R., Soya, S., & Sakurai, T. (2025). Q Neuron-Induced Hypothermia Promotes Functional Recovery and Suppresses Neuroinflammation after Brain Injury. *Journal of Neuroscience*, *45*(47). https://doi.org/10.1523/JNEUROSCI.1035-25.2025

Sato, K., Watamura, N., Fujioka, R., Mihira, N., Sekiguchi, M., Nagata, K., Ohshima, T., Saito, T., Saido, T. C., & Sasaguri, H. (2021). A third-generation mouse model of Alzheimer's disease shows early and increased cored plaque pathology composed of wild-type human amyloid β peptide. *Journal of Biological Chemistry*, *297*(3), 101004. https://doi.org/10.1016/j.jbc.2021.101004

Selkoe, D. J. (2002). Alzheimer's Disease Is a Synaptic Failure. *Science*, *298*(5594), 789–791. https://doi.org/10.1126/science.1074069

Selkoe, D. J., & Hardy, J. (2016). The amyloid hypothesis of Alzheimer's disease at 25 years. *EMBO Molecular Medicine*, *8*(6), 595–608. https://doi.org/10.15252/emmm.201606210

Shimohama, S., Fujioka, R., Mihira, N., Sekiguchi, M., Sartori, L., Joho, D., Saito, T., Saido, T. C., Nakahara, J., Hino, T., Hoshino, A., & Sasaguri, H. (2024). The Icelandic Mutation (APP-A673T) Is Protective against Amyloid Pathology In Vivo. *Journal of Neuroscience*, *44*(47). https://doi.org/10.1523/JNEUROSCI.0223-24.2024

Silva, I., Silva, J., Ferreira, R., & Trigo, D. (2021). Glymphatic system, AQP4, and their implications in Alzheimer's disease. *Neurological Research and Practice*, *3*(1), 5. https://doi.org/10.1186/s42466-021-00102-7

Singh, D. (2022). Astrocytic and microglial cells as the modulators of neuroinflammation in Alzheimer's disease. *Journal of Neuroinflammation*, *19*(1), 206. https://doi.org/10.1186/s12974-022-02565-0

Staples, J. F. (2014). Metabolic suppression in mammalian hibernation: The role of mitochondria. *Journal of Experimental Biology*, *217*(12), 2032–2036. https://doi.org/10.1242/jeb.092973

Storey, K. B., & Storey, J. M. (2010). Metabolic rate depression: The biochemistry of mammalian hibernation. *Advances in Clinical Chemistry*, *52*, 77–108.

Takahashi, T. M., Sunagawa, G. A., Soya, S., Abe, M., Sakurai, K., Ishikawa, K., Yanagisawa, M., Hama, H., Hasegawa, E., Miyawaki, A., Sakimura, K., Takahashi, M., & Sakurai, T. (2020). A discrete neuronal circuit induces a hibernation-like state in rodents. *Nature*, *583*(7814), 109–114. https://doi.org/10.1038/s41586-020-2163-6

Tarkowska, A., Furmaga-Jabłońska, W., Bogucki, J., Kocki, J., & Pluta, R. (2022). Hypothermia after Perinatal Asphyxia Does Not Affect Genes Responsible for Amyloid Production in Neonatal Peripheral Lymphocytes. *Journal of Clinical Medicine*, *11*(12), 3263. https://doi.org/10.3390/jcm11123263

Tsering, W., & Prokop, S. (2024). Neuritic Plaques—Gateways to Understanding Alzheimer's Disease. *Molecular Neurobiology*, *61*(5), 2808–2821. https://doi.org/10.1007/s12035-023-03736-7

Wang, J., Ho, L., Qin, W., Rocher, A. B., Seror, I., Humala, N., Maniar, K., Dolios, G., Wang, R., Hof, P. R., & Pasinetti, G. M. (2005). Caloric restriction attenuates β-amyloid neuropathology in a mouse model of Alzheimer's disease. *The FASEB Journal*, *19*(6), 1–18. https://doi.org/10.1096/fj.04-3182fje

Wang, X., Xie, Y., Chen, G., Lu, Y., Wang, D., & Zhu, L. (2023). Intermittent hypoxia therapy ameliorates beta-amyloid pathology via TFEB-mediated autophagy in murine

Alzheimer's disease. *Journal of Neuroinflammation*, *20*(1), 240. https://doi.org/10.1186/s12974-023-02931-6

Xie, L., Kang, H., Xu, Q., Chen, M. J., Liao, Y., Thiyagarajan, M., O'Donnell, J., Christensen, D. J., Nicholson, C., Iliff, J. J., Takano, T., Deane, R., & Nedergaard, M. (2013). Sleep Drives Metabolite Clearance from the Adult Brain. *Science*, *342*(6156), 373–377. https://doi.org/10.1126/science.1241224

Zhang, H., Ma, Q., Zhang, Y., & Xu, H. (2012). Proteolytic processing of Alzheimer's β-amyloid precursor protein. *Journal of Neurochemistry*, *120*(s1), 9–21. https://doi.org/10.1111/j.1471-4159.2011.07519.x

Zhou, F., Zhu, X., Castellani, R. J., Stimmelmayr, R., Perry, G., Smith, M. A., & Drew, K. L. (2001). Hibernation, a Model of Neuroprotection. *The American Journal of Pathology*, *158*(6), 2145–2151. https://doi.org/10.1016/S0002-9440(10)64686-X

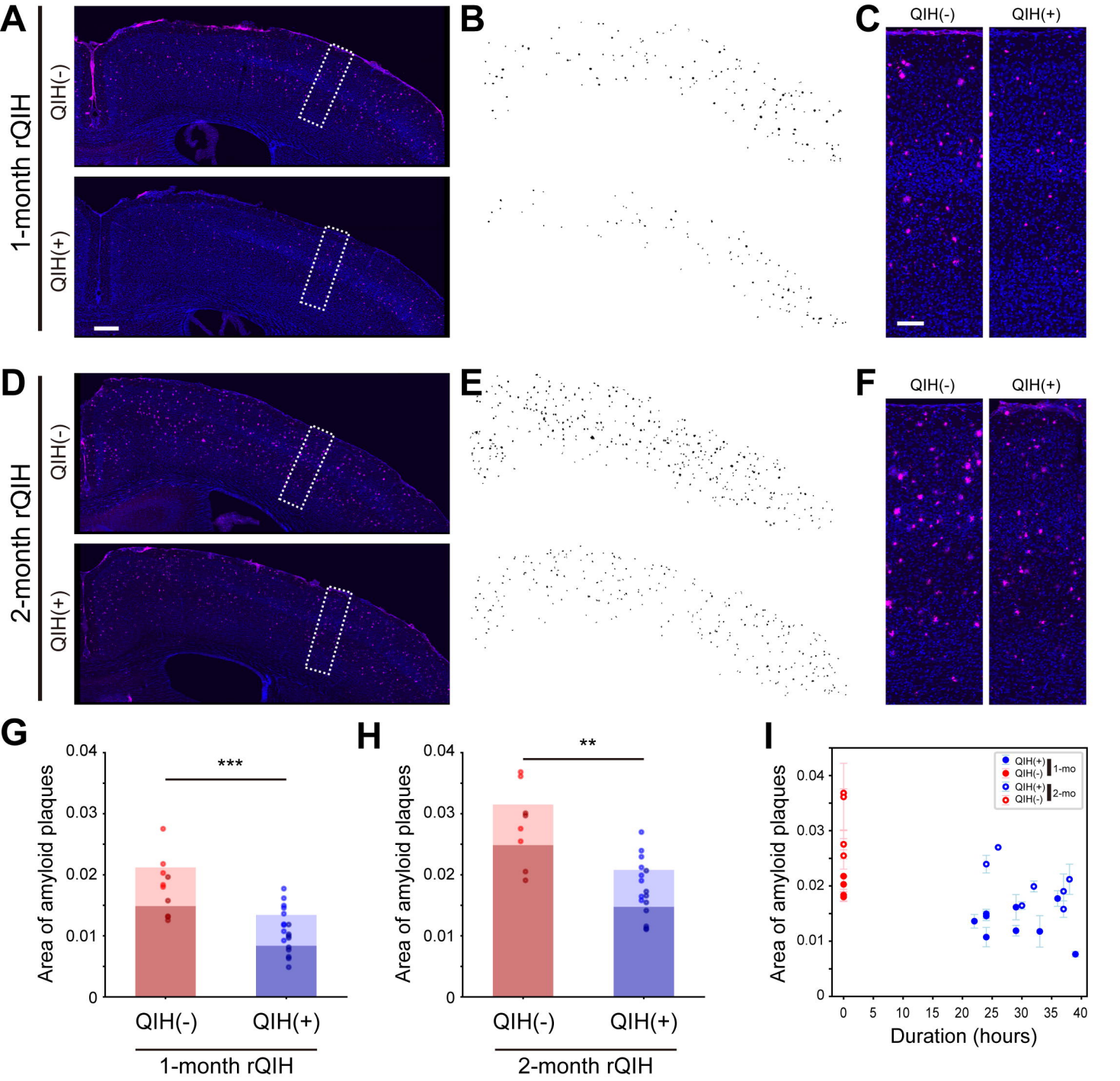
A
1-month rQIH
QIH(-)
QIH(+)
B
C
QIH(-)
QIH(+)
D
2-month rQIH
QIH(-)
QIH(+)
E
F
QIH(-)
QIH(+)
G
Area of amyloid plaques
0.04
0.03
0.02
0.01
0
***
QIH(-)
QIH(+)
1-month rQIH
H
Area of amyloid plaques
0.04
0.03
0.02
0.01
0
**
QIH(-)
QIH(+)
2-month rQIH
I
Area of amyloid plaques
0.04
0.03
0.02
0.01
0
QIH(+)
QIH(-)
1-mo
QIH(+)
QIH(-)
2-mo
0
5
10
15
20
25
30
35
40
Duration (hours)

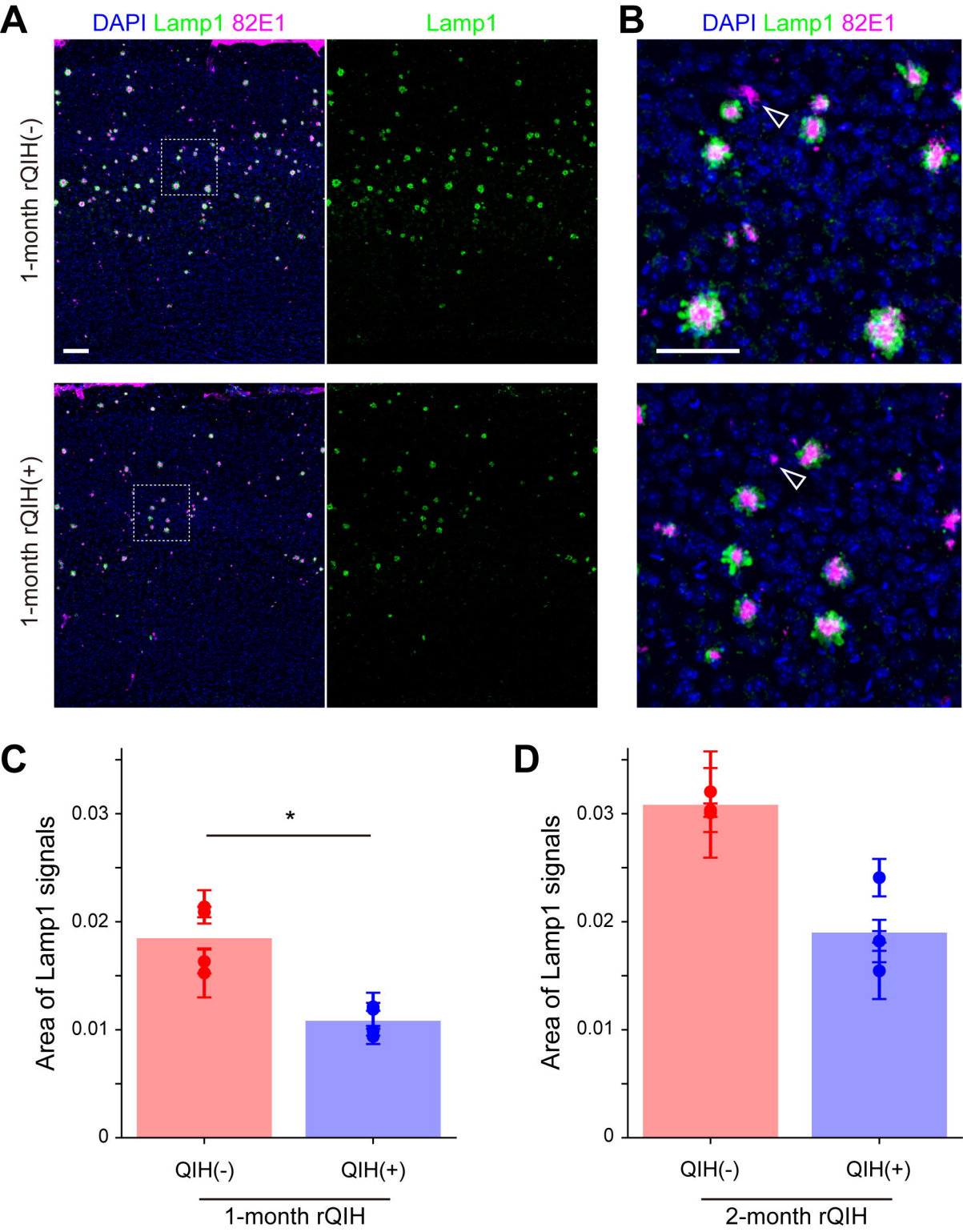
A
DAPI Lamp1 82E1
Lamp1
1-month rQIH(-)
1-month rQIH(+)
B
DAPI Lamp1 82E1
C
Area of Lamp1 signals
0.03
0.02
0.01
0
*
QIH(-)
QIH(+)
1-month rQIH
D
Area of Lamp1 signals
0.03
0.02
0.01
0
QIH(-)
QIH(+)
2-month rQIH

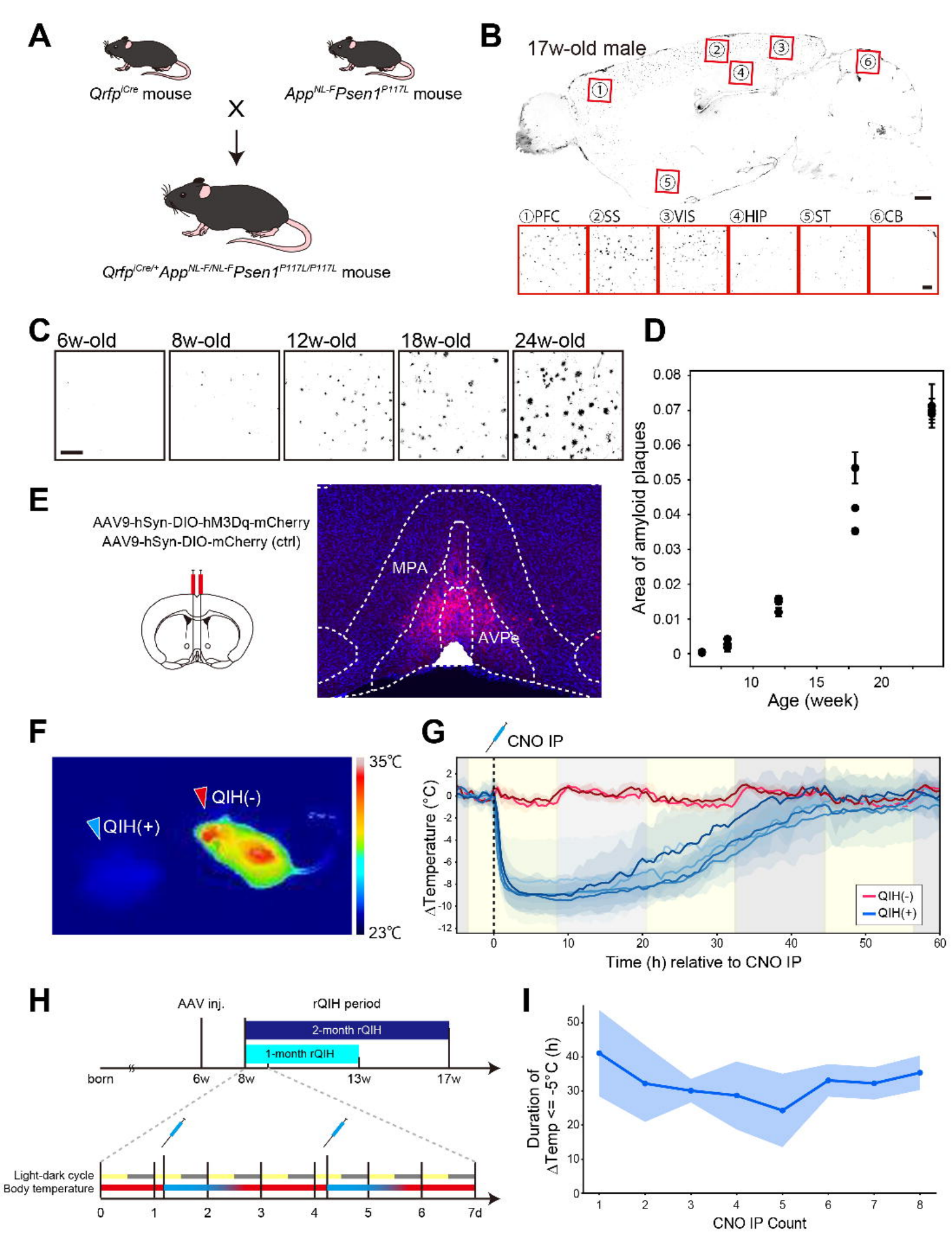
A
Qrfp^iCre mouse
App^NL-F Psen1^P117L mouse
X
Qrfp^iCre/+ App^NL-F/NL-F Psen1^P117L/P117L mouse
B
17w-old male
①PFC
②SS
③VIS
④HIP
⑤ST
⑥CB
C
6w-old
8w-old
12w-old
18w-old
24w-old
D
Area of amyloid plaques
Age (week)
E
AAV9-hSyn-DIO-hM3Dq-mCherry
AAV9-hSyn-DIO-mCherry (ctrl)
MPA
AVPe
F
QIH(-)
QIH(+)
35℃
23℃
G
CNO IP
ΔTemperature (°C)
Time (h) relative to CNO IP
QIH(-)
QIH(+)
H
AAV inj.
rQIH period
2-month rQIH
1-month rQIH
born
6w
8w
13w
17w
Light-dark cycle
Body temperature
7d
I
Duration of ΔTemp <= -5°C (h)
CNO IP Count